International Journal of Thermophysics, Vol. 28, No. 3, June 2007 (© 2007)
DOI: 10.1007/s10765-007-0192-0

Measurement and Modeling of the Emittance of Silicon Wafers with Anisotropic Roughness

H. J. Lee[1], A. C. Bryson[1], and Z. M. Zhang[1,2]

The unpolished surface of crystalline silicon wafers often exhibits non-Gaussian and anisotropic roughness characteristics, as evidenced by the side peaks in the slope distribution. This work investigates the effect of anisotropy on the emittance. The directional-hemispherical reflectance of slightly and strongly anisotropic silicon wafers was measured at room temperature using a center-mount integrating sphere. A monochromator with a lamp was used for near-normal incidence in the wavelength region from 400–1000 nm, and a continuous-wave diode laser at the wavelength of 635 nm was used for measurements at zenith angles up to 60°. The directional emittance was deduced from the measured reflectance based on Kirchhoff's law. The geometric-optics-based Monte Carlo model that incorporates the measured surface topography is in good agreement with the experiment. Both the experimental and modeling results suggest that anisotropic roughness increases multiple scattering, thereby enhancing the emittance. On the other hand, if the wafer with strongly anisotropic roughness were modeled as a Gaussian surface with the same roughness parameters, the predicted emittance near the normal direction would be lower by approximately 0.05, or up to 10% at a wavelength of 400 nm. Comparisons also suggest that the Gaussian surface assumption is questionable in calculating the emittance at large emission angles with *s* polarization, even for the slightly anisotropic wafer. This work demonstrates that anisotropy plays a significant role in the emittance enhancement of rough surfaces. Hence, it is imperative to obtain precise surface microstructure information in order to accurately predict the emittance, a critical parameter for non-contact temperature measurements and radiative transfer analysis.

[1] The George W. Woodruff School of Mechanical Engineering, Georgia Institute of Technology, Atlanta, Georgia, 30332, U.S.A.
[2] To whom correspondence should be addressed. E-mail zhuomin.zhang@me.gatech.edu

0195-928X/07/0600-0918/0 © 2007 Springer Science+Business Media, LLC

KEY WORDS: anisotropic roughness; emittance; integrating sphere; Monte Carlo method; reflectance.

1. INTRODUCTION

The variation of emittance due to surface roughness is a major concern in radiation thermometry [1,2]. Many researchers have studied the emittance of rough silicon surfaces for accurate radiometric temperature measurements during rapid thermal processing [3–5]. Vandenabeele and Maex [3] measured the emittance of wafers with varying degrees of surface roughness and found that even moderate roughness can enhance the emittance for wafers in the semitransparent spectral region. Furthermore, multiple reflections can enhance the emittance for opaque wafers with a large root-mean-square roughness.

Recent studies have showed that the slope distribution of roughness of silicon wafers is often non-Gaussian and anisotropic as a result of the chemical etching process [6]. Some wafers possess strong anisotropy as evidenced by side peaks in their slope distributions. Zhu and Zhang [6] incorporated the anisotropic slope distribution function, obtained from the topographic measurements made using an atomic force microscope (AFM), into an analytical model of the bidirectional reflectance distribution function (BRDF). Lee and Zhang [7] extended the model-based approach to silicon wafers with thin-film coatings and studied the combined effect of coating and anisotropic roughness on the BRDF. Using the Monte Carlo method, Lee et al. [8] developed ray-tracing techniques and obtained good agreement with measurements for both in-plane and out-of-plane BRDFs.

While anisotropic roughness affects the BRDF drastically, it is not clear whether the specific roughness statistics will have a large impact on the emittance, which is the integration of the BRDF over the hemisphere. Lee et al. [9] calculated the emittance of anisotropic silicon wafers and predicted an increase in emittance over that of a smooth surface or a Gaussian (isotropic) rough surface. In the present work, we present emittance measurements for silicon wafers with anisotropic roughness to study the effect of anisotropy on the directional spectral emittance with different polarizations. The results will be extensively compared with Monte Carlo models based on both the measured anisotropic surface topography and an assumed Gaussian surface with the same rms roughness (σ) and autocorrelation length (τ).

2. EXPERIMENT

This section first describes the samples and surface statistics, and then discusses the experimental setup used for measuring the radiative properties. Emphasis will be placed on the assumptions and corrections for the integrating sphere measurements.

The rough silicon samples, identified as Si-1 and Si-2, were prepared by dicing commercial lightly doped <100> single crystalline wafers into $25 \times 25\,\text{mm}^2$ pieces. The thickness of Si-1 is $525\,\mu\text{m}$, and that of Si-2 is $500\,\mu\text{m}$. These wafers have been extensively studied and described in Refs. [6, 8] . Their surface topographic data were measured several times using an AFM that scans over a $100 \times 100\,\mu\text{m}^2$ area and stores the output in a 512×512 data array. The roughness statistics were calculated from the measured topographic data to obtain the height and slope distribution functions. While the height distribution functions of the two samples appear to be very similar, the slope distribution functions of Si-1 and Si-2 are non-Gaussian and anisotropic. The anisotropy of Si-1 is not as striking as that of Si-2. The slope distribution function of Si-2 reveals eight side peaks (four large and four small) along diagonal directions, i.e., at the azimuthal angles $\phi = \pm 45°$, in addition to a central peak at zero slope. These side peaks are associated with the orientation of microfacets which has preferential orientation along the {311} and {111} crystalline planes, although some deviations exist due to the artifacts in the topographic measurements [6, 8]. The rms roughness σ of Si-1 is 0.51 μm, and that of Si-2 is $0.64\,\mu\text{m}$. The average rms slope w and autocorrelation length τ were calculated at $\phi = 0°$ and $\phi = 45°$ for each sample. However, the dependence on the azimuthal angle is negligibly small. The results are $w = 0.28$ and $\tau = 4.2\,\mu\text{m}$ for Si-1, and $w = 0.48$ and $\tau = 3.1\,\mu\text{m}$ for Si-2. Due to anisotropy, the relation $w = \sqrt{2}\sigma/\tau$, derived for Gaussian surfaces, does not hold anymore. It can be seen that the rms slope is much larger for Si-2 than for Si-1.

A custom-designed integrating sphere from Sphere Optics, Inc. was used to obtain the directional spectral emittance, by measuring the directional-hemispherical spectral reflectance. Figure 1 shows the experimental setup. The inner wall of the 200-mm-diameter sphere was coated with polytetrafluoroethylene (PTFE), which is a nearly diffuse material with a reflectance of approximately 0.99 in the wavelength region of interest [10]. A center-mount scheme was used in the present study for measurements at various angles of incidence [11, 12]. The entrance aperture has a diameter $D_e = 25\,\text{mm}$. A silicon detector was mounted at the bottom of the sphere with a baffle in front of it to block radiation directly from the sample. The sample can be rotated out of the beam path for a reference

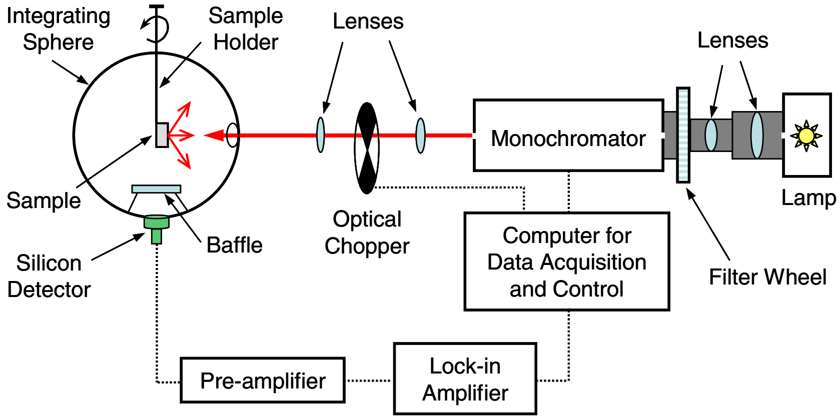

Fig. 1. Schematic of the setup for measuring spectral radiative properties. The light source consists of a tungsten halogen lamp, a filter wheel, and a monochromator. The light exiting the aperture of the monochromator is focused on the sample mounted in the middle of the integrating sphere. The light reflected by the sphere walls is collected by the silicon detector located at the bottom of the sphere under the baffle, which prevents direct reflection from the sample to the detector. The lock-in amplifier is used together with the pre-amplifier to pick up the detector output signals, which are synchronized with the frequency of an optical chopper.

measurement, in which light hits the back wall of the sphere. The sample measurement is taken by ensuring that all light hits the sample surface. The ratio of the signal from the sample measurement to that from the reference measurement allows the deduction of the directional-hemispherical reflectance as will be discussed later.

A monochromator (Oriel Instruments Cornerstone 130) with a tungsten halogen lamp served as the light source in the wavelength region from 400 to 1000 nm. The rms fluctuation of power from the monochromator was estimated to be less than 1%. Two lenses inside the light shield focus the emission from the lamp on the entrance slit of the monochromator, and the light from the exit slit has a focal length of 130 mm. The 1200 lines/mm grating provides a resolution of 10 nm at the wavelength of 500 nm when combined with entrance and exit slits of 1.56 mm width. In order to reduce the beam dimension, the exit slit was blocked above and below to confine the vertical opening to approximately 3.1 mm. Light passing through a collimating lens, which has a diameter of 25 mm and a focal length of 100 mm, and a chopper was then refocused to the sample by a second lens with a focal length of 250 mm. The beam-spot size on the sample was approximately $5 \times 10\,\text{mm}^2$. The chopper was synchronized to the lock-in amplifier (EG&G 7265DSP) at 400 Hz.

A thermoelectrically-cooled diode laser at the wavelength of 635 nm was used for reflectance measurements at different angles of incidence, because of its small beam size of approximately 3 mm diameter. Compared with the spectral power output from the monochromator, the continuous-wave diode laser can provide higher and more stable optical power, yielding much lower measurement noise. The incidence angle was determined by manual rotation of the sample holder. The lock-in amplifier was connected to the diode laser controller to supply modulated current, so that the optical power of the laser was modulated without using a mechanical chopper. A linear polarizer was placed between the diode laser and the integrating sphere to measure the reflectance for a specific polarization.

Inside the integrating sphere, light incident upon the sample or the sphere wall undergoes multiple reflections, and only a portion of the reflected power reaches the silicon detector. The detector output signal was sent to the lock-in amplifier, while passing through a trans-impedance pre-amplifier with a wide amplification range. The pre-amplifier gain was optimized so that the lock-in amplifier can efficiently pick up the phase-locked signal and filter out noise. Additional information about the diode laser system and electronics has been described in Ref. 13. Both the acquisition of data from the lock-in amplifier and the operation of the monochromator were digitally controlled under a LabView environment.

The reflectance of an opaque sample is calculated from the ratio of the radiant power reaching the detector when light is incident on the sample to that when light is incident on the sphere wall. When the incident beam with a radiant power Φ_{i} hits the sphere wall, the radiant power that reaches the detector after multiple reflections inside the sphere is

$$\Phi_{\mathrm{w}} = \frac{F R_{\mathrm{w}}}{1 - \overline{R}_{\mathrm{w}}} \Phi_{\mathrm{i}} \tag{1}$$

where R_{w} and $\overline{\mathrm{R}}_{\mathrm{w}}$ represent the reflectance of sphere wall and the average reflectance of the sphere wall, respectively. The view factor from the sphere wall to the detector is denoted by F. If the effects of the baffle, sample, and entrance aperture are neglected, then $F = D_{\mathrm{d}}^2/4D_{\mathrm{sp}}^2$, where D_{d} and D_{sp} stand for the diameters of the detector and the sphere, respectively [12, 14].

When the light is incident on the sample, the first reflection from the sample has a larger chance to escape from the entrance aperture than light from subsequent reflections. It is absolutely necessary to tilt the sample if the surface is smooth or has a large reflection peak. Even though the sample reflects diffusely, the view factor between the sample and the aperture

is roughly four times greater than that between the wall and the aperture because the sample is mounted at the center. Assuming that the rotation of the sample does not affect the average reflectance of the wall $\overline{R}_w$ and the view factor between the wall and the detector F, the total radiant power that reaches the detector for sample measurement is

$$\Phi_s = \frac{F R_s (1-\eta) R_w}{1-\overline{R}_w} \Phi_i \tag{2}$$

where R_s is the reflectance of the sample and η is the fraction of light leaving the sample directly through the entrance aperture. The term $(1-\eta) R_w$ represents the average reflectance of the wall that receives the first reflection from the sample. Although it is common practice to ignore the baffle, its effect has been considered in the derivation of Eq. (2) by assuming that the first reflection from the sample does not reach the detector directly [14].

If the detector sensitivity is independent of direction and the incoming power, the output signal will be proportional to the incoming radiant power. From Eqs. (1) and (2), the ratio of the detector outputs is related to the sample reflectance by

$$\frac{V_s}{V_w} = \frac{\Phi_s}{\Phi_w} = (1-\eta) R_s \tag{3}$$

which is the measurement equation of the integrating sphere. Theoretically, the correction factor η can be calculated from the BRDF $f_r(\theta_i, \phi_i, \theta_r, \phi_r)$, where θ and ϕ are the zenith and azimuthal angles and subscripts "i" and "r" signify incidence and reflection, respectively.

$$\eta = \frac{\int_{\omega_e} f_r(\theta_i, \phi_i, \theta_r, \phi_r) \cos\theta_r \mathrm{d}\omega_r}{\int_{2\pi} f_r(\theta_i, \phi_i, \theta_r, \phi_r) \cos\theta_r \mathrm{d}\omega_r} \tag{4}$$

The numerator represents the directional-conical reflectance from the sample toward the solid angle of the entrance aperture ω_e, while the denominator is the directional-hemispherical reflectance R_s. For a finite beam size, Eq. (4) needs to be integrated over the area as well, which is not done in the present study for simplicity. If the sample is specular, it is always possible to tilt the sample so that the first reflection hits the wall rather than the aperture. In this case, $\eta = 0$ and no correction is needed. For a diffuse sample, η is reduced to the view factor from the sample to the entrance aperture as $\eta = D_e^2/(D_e^2 + D_{sp}^2) = 0.015$. The samples of interest are however, neither specular nor diffuse, and the calculation of η and the measurement uncertainty will be discussed later.

Although the derivation of Eq. (3) is based on opaque samples, this measurement equation can be used for emittance measurements of semitransparent materials by replacing the right side of Eq. (3) with $(1-\eta)R_\mathrm{s} + T_\mathrm{s} = R_\mathrm{s} + T_\mathrm{s} - \eta'$, where $\eta' = \eta R_\mathrm{s}$ is a new correction factor that is equal to the numerator of Eq. (4). Hence, the ratio of the detector outputs gives the sum of reflectance and transmittance. The directional spectral emittance can be calculated by $\varepsilon'_\lambda = 1 - R_\mathrm{s} - T_\mathrm{s}$ according to Kirchhoff's law. In terms of emittance, the direction defined by $(\theta_\mathrm{i}, \phi_\mathrm{i})$ becomes the direction of emission; therefore, θ_i and ϕ_i are called the emission angles. All measurements in the present study were performed at room temperature.

3. MONTE CARLO MODELING

If a surface is rough, multiple reflections can occur in cavities formed by roughness. As a result, surface roughness traps incident light in the cavities, thereby increasing absorptance or emittance. When a material is semitransparent, the emittance can increase drastically due to the large chance of light trapping by total internal reflections inside the material. Some previous studies calculated the emittance of rough silicon wafers by considering surface roughness as a parameter in an emittance model without considering the actual statistics of the surface topography [3,4]. In the present study, we calculate the emittance from the BRDF obtained from a Monte Carlo ray-tracing method, which incorporates the actual surface statistics to investigate the effect of anisotropic roughness on the directional spectral emittance. When geometric optics is applicable, the Monte Carlo method takes full account of multiple scattering and allows the prediction of emittance enhancement due to the cavity effects that cause light trapping.

From the viewpoint of geometric optics, a rough surface consists of many small, smooth surfaces called microfacets. In the Monte Carlo method, a large number of rays are traced numerically between microfacets while undergoing reflections [8,9,15–17]. Incident light rays are specularly reflected at each microfacet, and the energy of the ray is reduced by the locally calculated reflectivity. The rays are traced for multiple reflections at the surface until they leave the surface without restriking. Most ray-tracing methods use a pre-generated rough surface, which is constructed before the ray bundles are traced. The numerical generation of a rough surface is called a surface realization. A surface realization provides a discrete surface profile, from which the direction of reflection and the reflectivity can be determined based on the physical location and orientation of a microfacet. The BRDF of a surface

realization is calculated with an algebraic sum of the reduced energy of rays leaving in the same direction, and BRDFs are averaged with a sufficiently large number of surface realizations to suppress statistical fluctuations. Moreover, the calculation of the directional-conical reflectance using the Monte Carlo method is straightforward if the solid angle of a reflection cone is specified. Therefore, the directional-hemispherical reflectance can be simultaneously calculated based on the numerical algorithm. Furthermore, the Monte Carlo method also yields the correction factor η in Eq. (4) based on the solid angle between the surface and the entrance aperture for given surface statistics and optical constants of the sample.

The spectral method based on the power spectrum and random numbers is widely applied for surface realizations [15]. Since the power spectrum is obtained from the variance σ^2 and the autocorrelation function using the Fourier transform, a rough surface is commonly specified with rms roughness σ and autocorrelation length τ, by prescribing an autocorrelation function. For instance, a Gaussian surface is generated with the Gaussian autocorrelation function once values of σ and τ are specified. However, the spectral method is not applicable for the generation of anisotropic surfaces although the variance and the autocorrelation function of the anisotropic surfaces can be obtained from surface topographic measurements. Lee et al. [8] performed ray tracing on the surface profile that the AFM measurement provides as a two-dimensional (2D) array. Direct ray tracing with the surface topography measurement allows the incorporation of actual surface statistics into modeling.

The consideration of depolarization is necessary to model the emittance of a 2D rough surface for s or p polarization. Even though the incident light is purely s or p polarized, both polarization components are present in the local coordinates of a microfacet due to its random orientation. As a result, the polarization state of the scattered wave is different from that of the incident wave, i.e., depolarization occurs. Depolarization can be considered in the ray-tracing algorithm when Fresnel's reflection coefficients are calculated [8]. In the present study, the emittance is calculated for each polarization of the incident wave, taking into account depolarization. The emittance can be determined for each individual polarization, assuming that Planck's blackbody distribution function is divided by two to describe an equilibrium photon gas for a single polarization. This will allow the definition of emittance for each polarization to lie between 0 and 1. On the other hand, the average of the emittance for p and s polarizations gives the emittance with both polarization components. This is the regular emittance defined according to Planck's law considering both polarizations. Kirchhoff's law is applicable for each

polarization individually. Since the reflectance for random polarization is the average of the reflectance for p and s polarizations, the regular emittance is one minus the reflectance for random polarization for opaque surfaces. When the radiative properties of isotropic surfaces for random polarization are of interest, many studies assumed that changes between p and s polarizations counterbalance each other due to randomness of the scattering events, and thus ignored depolarization [16,17]. However, this approximation may not be applicable to anisotropic surfaces, for which depolarization may be significant, even for random polarization.

4. RESULTS AND DISCUSSION

The measurement equation, i.e., Eq. (3), inevitably causes errors in actual measurements because of the assumptions made in the integrating sphere theory. General error sources for integrating sphere measurements have been identified and well documented [11,12]. In particular, Edwards [11] carefully examined various error sources for center-mount integrating spheres. In the present study, measurements were made on a double-side-polished silicon wafer to estimate the uncertainty, as discussed next.

The wafer with both sides polished is lightly doped single crystalline silicon of 200 μm thickness. The spectral measurements were made using the monochromator, with the sample tilted at approximately 7°. No polarizer was used because the difference between the two polarizations is negligible at this angle. Figure 2a shows the emittance averaged over five measurements, along with that calculated using the optical constants of silicon given in Ref. [18]. For a smooth sample, $\eta = 0$ and no correction in the measurement equation is necessary. The wafer is opaque except near the wavelength $\lambda = 1000$ nm, where the emittance drops suddenly because the wafer becomes semitransparent. The reduction of the emittance at short wavelengths is due to an increase in the refractive index of silicon. Excellent agreement exists between the experiment and calculation with the largest deviation of 0.008 occurring at 950 nm. Standard deviations for five measurements are less than 0.001. Based on both the 95% confidence level of five measurements and the deviation from the calculations, the expanded uncertainty for measurements of near-normal emittance is estimated to be less than 0.010.

Figure 2b shows the emittance of the double-side-polished wafer at different emission angles, measured using the 635 nm diode laser for each polarization. The measured data points are indicated by symbols: circles are for p polarization and diamonds for s polarization. The theoretical calculations are shown as curves for comparison. The maximum standard deviation of five measurements increases to 0.005 due to manual rotation

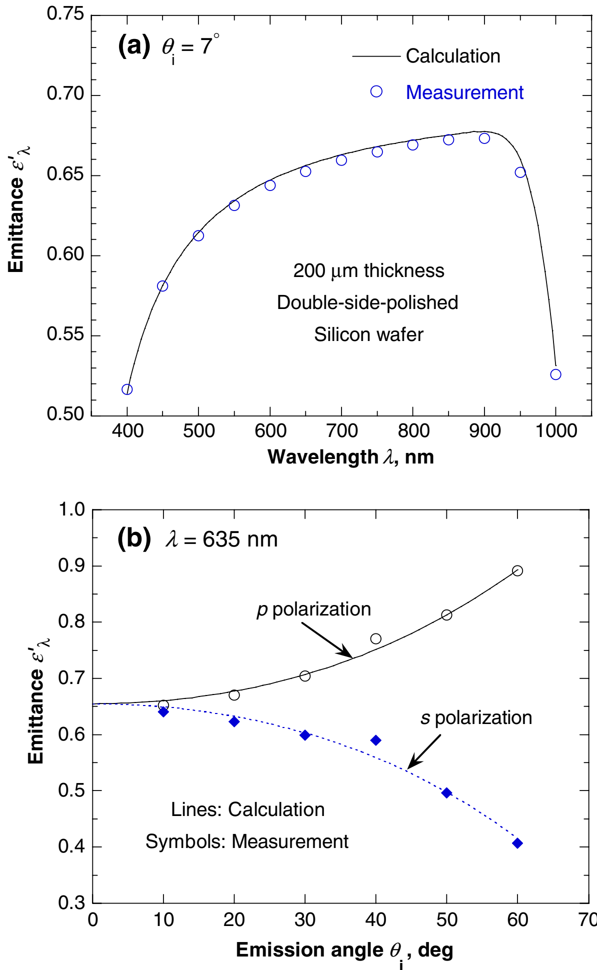

Fig. 2. Comparison of emittance measurements (circle or diamond symbols) with theoretical calculations (solid or dashed line) for a double-side-polished wafer of 200 μm thickness: (a) emittance spectrum for the near-normal direction ($\theta_i \approx 7°$) in the wavelength region from 400 to 1000 nm; and (b) variation of emittance with the emission angle θ_i at the wavelength of 635 nm for individual polarizations.

of the sample holder. Except at the emission angle of 40°, deviations of measurements are less than 0.008, which are comparable to those of the monochromator measurement shown in Fig. 2a. Much larger deviations occur at $\theta_i = 40°$, where the absolute error becomes 0.020 for p polarization and 0.032 for s polarization. A rod supporting the baffle lies between

a sidewall of the sphere and the detector; refer to Fig. 1. Therefore, when the incidence angle is around 45°, the support rod screens some of the reflected light from the sidewall to the detector, resulting in large measurement errors. However, if a rough sample is measured, the errors due to the support rod will be reduced. Therefore, the expanded uncertainty for directional measurements is estimated to be generally within 0.020.

The measured emittance spectrum of Si-1 for random polarization in the near-normal direction is shown in Fig. 3a, together with modeling results from two different methods. Recall that Si-1 is a rough surface with slight anisotropy. Anisotropic modeling was based on the AFM topographic measurements. Gaussian modeling was based on hypothetical Gaussian surface realizations generated by the spectral method with the same rms roughness and autocorrelation length as those of the rough surface. The two modeling methods reveal negligibly small deviation in the predicted emittance of Si-1. Both modeling results agree with experiment well within an expanded uncertainty of 0.010, except at the wavelength of 1000 nm. As mentioned earlier, while the wafer is essentially opaque at wavelengths shorter than 950 nm, it becomes slightly transparent at $\lambda = 1000$ nm even with a thickness of 500 μm. The ray-tracing model was based on opaque surfaces, but the integrating sphere collected both the reflected and transmitted radiation. For this reason, the calculation overpredicts the emittance at $\lambda = 1000$ nm. The results shown in Fig. 3a suggest that the emittance enhancement due to roughness is insignificant for Si-1. Specifically, the increase in emittance of Si-1 is less than 0.8% over that of a smooth surface in the opaque region.

The anisotropic modeling shows that the correction factor η for Si-1 at $\theta_i = 7°$ does not change significantly with wavelength, and thus a constant value of 0.035 has been applied for the measurements in Fig. 3a. The correction factor changes the absolute values of emittance by 0.012 (relatively 1.9%) on the average. Emittance measurements would change by 0.005 under the assumption of diffuse reflection ($\eta = 0.015$). The difference in measurements using the two values of the correction factor is within the experimental uncertainty. If the Gaussian surface model were used, the correction factor would be 0.055, which could change measurements by 0.020. Obviously, the correction factor based on anisotropic BRDF modeling is more reasonable.

Figure 3b shows a similar comparison for the emittance of Si-2 at wavelengths from 400 to 1000 nm. The correction factor η for all measurements of Si-2 can be approximated as 0.024, which is closer to the correction factor for a diffuse surface. Gaussian modeling yields essentially the same value of η for Si-2. The standard deviation of the anisotropic modeling results is approximately 0.008 due to the artifacts of AFM

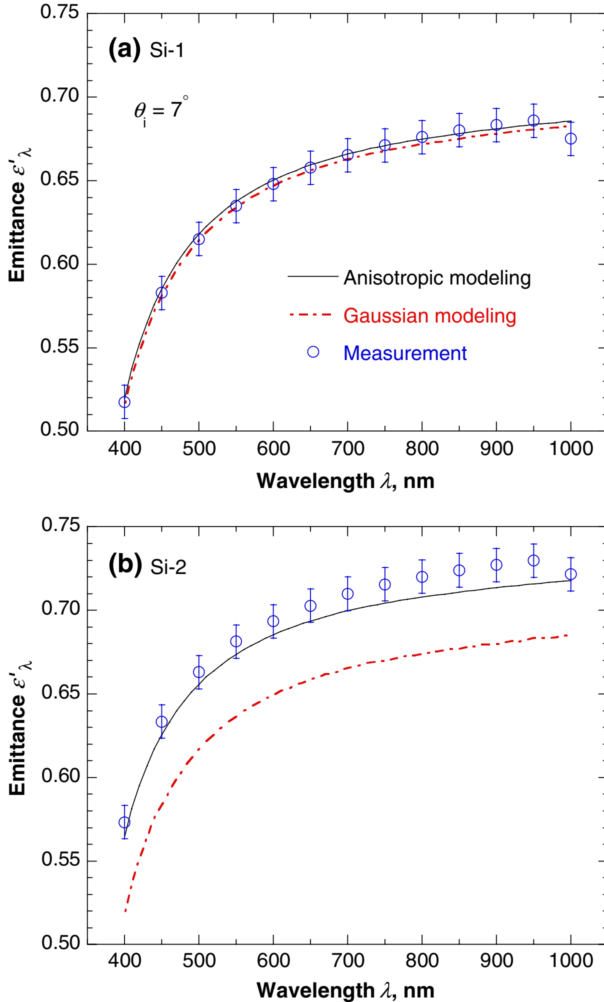

Fig. 3. Comparison of the measured and predicted near-normal emittance for the two rough wafers: (a) Si-1 and (b) Si-2. The anisotropic modeling relies on the measured surface topographic data, whereas the Gaussian modeling assumes that the surfaces follow Gaussian statistics with corresponding roughness parameters σ and τ. Error bars indicate measurement uncertainty.

measurements for Si-2 [8]. It can be seen that Si-2 gives rise to a noticeable enhancement of emittance, compared to the emittance of a smooth surface in Fig. 2a. The average enhancement is 0.050 (7.8%), and the maximum is 0.058 (11.3%) at 400 nm. While anisotropic modeling is in

reasonable agreement with experiments, Gaussian modeling failed to predict the emittance enhancement. These striking results are further discussed below.

Anisotropic modeling predicts well the large emittance enhancement for Si-2, but the prediction is consistently lower than the measurements. The standard deviation between the anisotropic modeling and the measurement is 0.010 (absolute) or 1.5% (relative), which slightly exceeds the uncertainty of the integrating sphere measurements. This disagreement may be due to artifacts in the AFM surface measurements and to the limitations of geometric optics. The absolute deviation between the anisotropic modeling and experiment increases slightly with the wavelength. The reflectance, on the other hand, decreases with increasing wavelength. Therefore, the relative difference between the predicted and measured reflectance increases from 2% to 5% as the wavelength is increased from 400 to 950 nm. Geometric optics is applicable when the wavelength is much smaller than the autocorrelation length ($\tau = 3.1\ \mu$m for Si-2). Considering the uncertainty of integrating sphere and surface measurements, it can be concluded that geometric optics is valid for Si-2 in predicting the emittance. This result is consistent with the recent study on the applicability of geometric optics in modeling the emittance of rough surfaces [19].

Unlike anisotropic modeling, Gaussian modeling underpredicts the emittance of Si-2 by 7% on the average with a maximum of 10% at $\lambda =$ 400 nm. The emittance enhancement of the Gaussian surface is insignificant, similarly to the emittance of Si-1 shown in Fig. 3a. The large difference between the two modeling results occurs due to the effect of the strong anisotropy of the Si-2 roughness. The average inclination angle of microfacets on the Gaussian surface is 9.7° from the relation of $\sqrt{2}\sigma/\tau$. However, the large and small side peaks in the slope distribution function of Si-2 indicate that Si-2 possesses a larger number of steep microfacets inclined at 25.2° and 54.7° than does the Gaussian surface. Thus, the steep microfacets of Si-2 strengthen the cavity effects to trap incident light by multiple scattering, and the resulting large enhancement cannot be predicted with Gaussian surface statistics. It can be concluded that anisotropic roughness is the reason for the emittance enhancement for Si-2. Therefore, detailed information on the roughness statistics is essential for accurate prediction of the emittance of anisotropic surfaces.

Figure 4 shows the variation of emittance with emission angles for Si-1 and Si-2, at the wavelength of 635 nm, measured with the diode laser. To examine the effect of the azimuthal angle for anisotropic surfaces, the emittance for each polarization was measured along both the x axis ($\phi_{\mathrm{i}} = 0°$) and the diagonal ($\phi_{\mathrm{i}} = 45°$). The correction factor η depends considerably on the zenith angle θ_{i}. Approximate values of η for

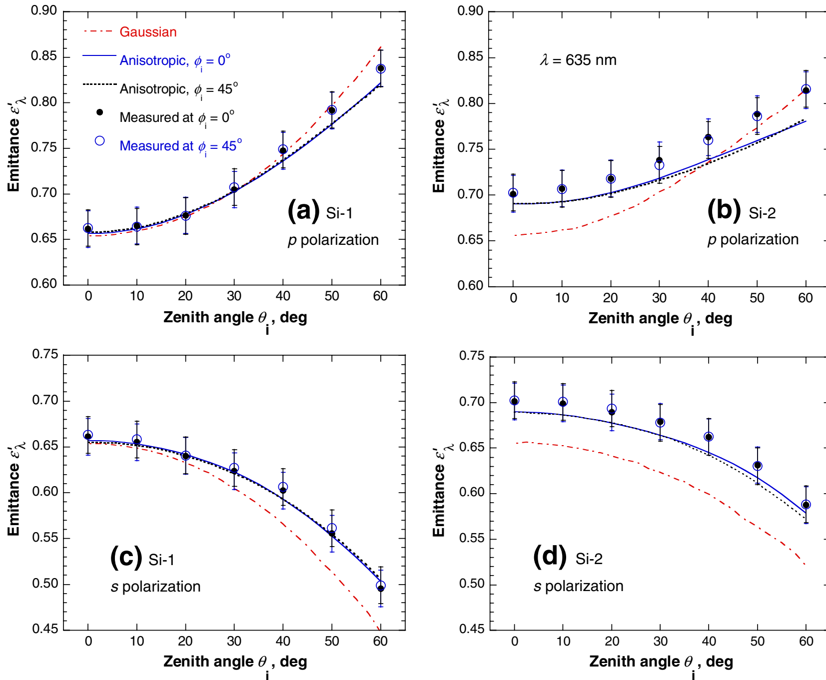

Fig. 4. Emittance of the two rough silicon wafers measured at the wavelength of 635 nm for two azimuthal angles $\phi_i = 0°$ and $\phi_i = 45°$: (a) Si-1, *p* polarization; (b) Si-2, p polarization; (c) Si-1, *s* Si-2,*p* polarization; and (d) *s* polarization.

measurements of Si-1 are 0.065, 0.025, and 0.015 at $\theta_i = 0°$, 10°, and 20°, respectively, and they become almost zero at larger angles. The values of of η for measurements of Si-2 are 0.058 and 0.013 at $\theta_i = 0°$ and 10°, respectively, and negligible at larger angles.

Comparisons for Si-1 in Fig. 4a, c show that the anisotropic modeling agrees well with measurement, although slight disagreement is observed at angles beyond $\theta_i = 40°$. This disagreement may be related to the blocking of light by the rod that supports the baffle, as demonstrated in Fig. 2b. The Monte Carlo model based on geometric optics may be subject to larger uncertainties at large angles. The standard deviation between the anisotropic modeling and the measurement is 0.008. The dependence on azimuthal angle is negligible for Si-1 in accordance with the slightly anisotropic slope distribution function. On the other hand, Gaussian modeling tends to deviate from measurement at large angles, especially for *s* polarization.

As demonstrated previously [6, 8], the anisotropy of Si-2 is so strong that the BRDF of Si-2 along $\phi_i = 45°$ reveals prominent side peaks according to the slope distribution function, whereas no side peaks exist in the BRDF along $\phi_i = 0°$. However, the measured and predicted emittance values are close to each other between $\phi_i = 0°$ and $\phi_i = 45°$, as shown in Fig. 4b, d. It appears that the effect of anisotropy on the emittance evens out in the azimuthal direction as a result of the integration of BRDF. In a trend similar to that shown in Fig. 3b, anisotropic modeling consistently underpredicts the emittance, and the difference gradually increases with θ_i for p polarization. The standard deviation between the anisotropic modeling and the measurement is 0.021 for Si-2. However, the Gaussian modeling does not predict the variation of emittance for p polarization correctly and largely underpredicts the emittance for s polarization.

When the emittance of Si-1 and Si-2 shown in Fig. 4 is compared to that of a smooth silicon surface (e.g., Fig. 2b), the emittance for p polarization is decreased at large angles, while that for s polarization is increased. This can be explained by the effect of depolarization, which becomes significant at large θ_i. Furthermore, depolarization affects the emittance of Si-2 more strongly than that of Si-1 due to larger surface roughness. Consequently, the emittance difference between the two polarizations is much smaller for Si-2. However, the average emittance for the two polarizations depends little on θ_i, indicating nearly diffuse emission up to 60° for both Si-1 and Si-2, similar to that of a smooth surface.

5. CONCLUSIONS

The directional spectral emittance of two silicon wafers with slightly and strongly anisotropic roughness was measured using a center-mount integrating sphere at wavelengths from 400 to 1000 nm. The Monte Carlo method was used to predict the emittance based on measured surface topography. The results suggest that anisotropic roughness can significantly enhance the emittance due to the increased cavity effects for light trapping. As a result, the simple assumption of a Gaussian surface yields errors as large as 10% at 400 nm and 7% on the average for the strongly anisotropic wafer. Even for the slightly anisotropic wafer, the emittance modeled with Gaussian statistics deviates at large angles. Furthermore, the consideration of depolarization in the modeling is important to accurately predict the angular dependence of the emittance for p and s polarizations. The present study manifests the significant role of anisotropic roughness in the enhancement of emittance and illustrates pitfalls of assuming Gaussian surfaces without addressing specific roughness statistics. Therefore, precise

measurements and appropriate incorporation of surface topography in the modeling are critical for accurate prediction of the emittance.

ACKNOWLEDGMENTS

This work was supported by the National Science Foundation (CTS-0500113). The authors thank Dr. Y.-B. Chen of the Georgia Institute of Technology for assistance in the experimental setup and Dr. L. M. Hanssen of the National Institute of Standards and Technology for helpful discussions about integrating sphere measurements.

REFERENCES

1. D. P. DeWitt and G. D. Nutter, *Theory and Practice of Radiation Thermometry* (Wiley, New York, 1988).
2. Z. M. Zhang, *Annual Review of Heat Transfer*, Vol. 11 (Begell House, New York, 2000), p. 351.
3. P. Vandenabeele and K. Maex, *J. Appl. Phys*. **72**:5867 (1992).
4. N. M. Ravindra, B. Sopori, O. H. Gokce, S. X. Cheng, A. Shenoy, L. Jin, S. Abedrabbo, W. Chen, and Y. Zhang, *Int. J. Thermophys.* **22**:1593 (2001).
5. B. K. Tsai, D. P. DeWitt, E. A. Early, L. M. Hanssen, S. N. Mekhontsev, M. Rink, K. G. Kreider, B. J. Lee, and Z. M. Zhang, in *Proc. Tempmeko 2004*, Vol. 2 (Cavtat-Dubrovnik, Croatia, 2004), p. 1179.
6. Q. Z. Zhu and Z. M. Zhang, *Opt. Eng.* **44**:073601 (2005).
7. H. J. Lee and Z. M. Zhang, *Int. J. Thermophys.* **27**:820 (2006).
8. H. J. Lee, Y. B. Chen, and Z.M. Zhang, *Int. J. Heat Mass Transfer* **49**:4482 (2006).
9. H. J. Lee, Q. Z. Zhu, and Z. M. Zhang, in *Proc. 38th AIAA Thermophys. Conf.* AIAA (Toronto, Canada, 2005) AIAA-2005-5209.
10. V. R. Weidner and J. J. Hsia, *J. Opt. Soc. Am.* **71**:856 (1981).
11. D. K. Edwards, J. T. Gier, K. E. Nelson, and R. D. Roddick, *J. Opt. Soc. Am.* **51**:1279 (1961).
12. L. M. Hanssen and K. A. Snail, *Handbook of Vibrational Spectroscopy*, Vol. 2 (Wiley, New York, 2002), p. 1.
13. Y. J. Shen, Q. Z. Zhu, and Z. M. Zhang, *Rev. Sci. Instrum.* **74**:4885 (2003).
14. L. M. Hanssen, *Appl. Optics* **28**:2097 (1989).
15. E. I. Thorsos, *J. Acoust. Soc. Am*. **83**:78 (1988).
16. K. Tang and R. O. Buckius, *Int. J. Heat Mass Transfer* **41**:2037 (1998).
17. H. J. Lee, B. J. Lee, and Z. M. Zhang, *J. Quant. Spectrosc. Radiat. Transfer* **93**:185 (2005).
18. B. J. Lee, Z. M. Zhang, E. A. Early, D. P. DeWitt, and B. K. Tsai, *J. Thermophys. Heat Transfer* **19**:558 (2005).
19. F. Ghmari, I. Sassi, and M. S. Sifaoui, *Waves Random Complex* **15**:469 (2005).